Mpox virus infection and drug treatment modelled in human skin organoids

Li, P.F.; Pachis, S.T.; Xu, G.G.; Schraauwen, R.; Incitti, R.; Vries, A.C. de; ... ; Pan, Q.W.

nature microbiology

Article

https://doi.org/10.1038/s41564-023-01489-6

Mpox virus infection and drug treatment modelled in human skin organoids

Received: 3 February 2023

Accepted: 4 September 2023

Published online: 12 October 2023

Check for updates

Pengfei Li[1,7], Spyridon T. Pachis[2,3,7], Guige Xu[1], Rick Schraauwen[4], Roberto Incitti[5], Annemarie C. de Vries[1], Marco J. Bruno[1], Maikel P. Peppelenbosch[1], Intikhab Alam[5], Karine Raymond[2,3,6,8] ✉ & Qiuwei Pan[1,8] ✉

Mpox virus (MPXV) primarily infects human skin to cause lesions. Currently, robust models that recapitulate skin infection by MPXV are lacking. Here we demonstrate that human induced pluripotent stem cell-derived skin organoids are susceptible to MPXV infection and support infectious virus production. Keratinocytes, the predominant cell type of the skin epithelium, effectively support MPXV infection. Using transmission electron microscopy, we visualized the four stages of intracellular virus particle assembly: crescent formation, immature virions, mature virions and wrapped virions. Transcriptional analysis showed that MPXV infection rewires the host transcriptome and triggers abundant expression of viral transcripts. Early treatment with the antiviral drug tecovirimat effectively inhibits infectious virus production and prevents host transcriptome rewiring. Delayed treatment with tecovirimat also inhibits infectious MPXV particle production, albeit to a lesser extent. This study establishes human skin organoids as a robust experimental model for studying MPXV infection, mapping virus–host interactions and testing therapeutics.

Mpox virus (formerly monkeypox virus; MPXV) is the aetiological pathogen of mpox disease in humans. It is a large double-stranded DNA virus, belonging to the genus Orthopoxvirus of the family *Poxviridae*[1]. Over past decades, MPXV endemically circulates in tropical regions of African countries, predominantly in Central Africa[2]. However, in 2022, multi-national mpox outbreaks emerged across non-endemic regions spreading to over 100 countries, with the majority of infected cases reported in Europe and Americas[3,4].

Mpox disease is milder than that of smallpox, which is caused by variola virus, another member of the Orthopoxvirus genus. However, severe complications and even death have been reported in both previous outbreaks and the 2022 mpox outbreak, especially in vulnerable populations including young children, pregnant women and immunocompromised individuals[5]. Skin lesions are the most common symptom, which often appear on the face and extremities. However, lesions located in the genital–perianal areas of infected patients were commonly reported in the 2022 outbreak[3,6]. Although these lesions usually result in mild itches or aches with limited distribution across the body, during the 2022 outbreak there were frequent reports of more severe pain, systemic distribution and secondary infection of bacteria in the skin[7–9]. Close contact with MPXV-infected skin lesions is a major route of human-to-human transmission; therefore, there is an urgent need for better understanding of the pathophysiology of MPXV infection in this site and rapid development of therapeutics.

[1]Department of Gastroenterology and Hepatology, Erasmus MC-University Medical Center, Rotterdam, the Netherlands. [2]Department of Anatomy and Embryology, Leiden University Medical Center, Leiden, the Netherlands. [3]The Novo Nordisk Foundation Center for Stem Cell Medicine (reNEW), Leiden University Medical Center, Leiden, the Netherlands. [4]Department of Pathology, Erasmus MC-University Medical Center, Rotterdam, the Netherlands. [5]Computational Bioscience Research Center, King Abdullah University of Science and Technology, Thuwal, Saudi Arabia. [6]University of Grenoble Alpes, CEA, Inserm, IRIG, UA13 BGE, Biomics, Grenoble, France. [7]These authors contributed equally: Pengfei Li, Spyridon T. Pachis. [8]These authors jointly supervised this work: Karine Raymond, Qiuwei Pan. ✉e-mail: k.i.raymond@lumc.nl; q.pan@erasmusmc.nl

This in turn requires robust experimental models that can closely mimic skin features. Currently available in vitro models of MPXV infection are exclusively based on immortalized cell lines, which do not fully recapitulate human skin. A number of animal models have been developed for MPXV infection, but they usually do not develop the skin manifestations seen in humans[10].

Human induced pluripotent stem (hiPS) cell-derived skin organoids are capable of reproducing key physical and physiological characteristics of human skin. These 3D cultured organoids display a multilayer structure with an inverted configuration, meaning that, in contrast to in vivo skin, the dermis is in contact with the external environment while the epidermis is facing inwards towards the centre of the organoid. They also bear multiple appendages such as hair follicles and sebaceous glands[11]. Furthermore, a recently described approach utilizes an air–liquid interface (ALI) culture system that allows skin organoid maturation to occur in a manner that more closely resembles human skin physiology[12]. In this system, skin organoids are dissected and subsequently grown on a collagen-coated transwell so that the dermal layer is in contact with the culture medium whereas the epidermis is exposed to the air. Collectively, these features endow skin organoids with unique advantages for studying skin-associated diseases, microbial infection and drug development[13,14]. In this Article, we address whether hiPS cell-derived skin organoids might provide a robust model system in which to study MPXV pathogenesis in the skin and test antiviral treatment. We found that hiPS cell-derived skin organoids support productive infection of MPXV. Infection results in abundant expression of viral transcripts and rewires the host transcriptome. Treatment with the antiviral drug tecovirimat inhibits infectious MPXV particle production, demonstrating the potential of this model system for mapping virus–host interactions and testing antiviral treatments.

Results

MPXV infection in early-stage skin organoids

To investigate whether human skin organoids are permissive to MPXV infection, we inoculated intact skin organoids at different stages of maturity with a patient-derived MPXV isolate from the 2022 outbreak. As a first test, we used skin organoids at day 55 of differentiation (Fig. 1a). At this stage, the epithelium of skin organoids has not fully stratified but consists of basal keratinocytes that express both keratin 5 (KRT5) and keratin 15 (KRT15), an intermediate layer with low levels of KRT5, and a periderm-like outer layer with high levels of KRT15 (ref. 15). We tested organoids derived from two different lines of hiPS cells originated from healthy donors, and observed 3 $\log_{10}$ increase in intracellular viral genome copies at 7 days compared with 1 h post-inoculation in both lines (Fig. 1b). The kinetics of extracellular virus secreted into culture medium, from 1 h, 1 day and up to 7 days post-inoculation, showed a continuous increase in viral DNA levels and peaked at around 9 $\log_{10}$ copies ml^{-1} medium (Fig. 1c). This corresponds to an increase of infectious titres from approximately 1.5–2 $\log_{10}$ plaque-forming units (PFU) ml^{-1} at 1 h to 3.7 $\log_{10}$ PFU ml^{-1} at 7 days post-inoculation (Fig. 1d). Similarly, intracellular infectious viral titres from organoids increased from 1 h to 7 days post-inoculation (Extended Data Fig. 1a). Since the infection kinetics of these two independent lines is identical, our following experimentations and results with three different lines of hiPS cells were pooled for analysis.

The infection was visualized by immunostaining viral replicating intermediate double-stranded RNA (dsRNA) in cryosections of infected skin organoids. Co-localization of dsRNA, KRT5 and KRT15 demonstrated the infection in keratinocytes (Fig. 1e). Transmission electron microscopy (TEM) visualized the intracellular MPXV particles, with the majority captured at the immature and mature virion stages (Fig. 1f,g). Several intermediate assembly steps, such as immature virion packaging by dense membrane and the transition form before mature virions, were observed (Fig. 1h).

MPXV infection in late- and end-stage skin organoids

Next, skin organoids differentiated for 90 days were tested for the susceptibility to MPXV infection (Fig. 2a). Skin organoids at this later developmental stage display a stratified epithelium with a differentiated outer layer expressing loricrin and FLG, and pronounced hair peg formation[11,12]. We observed an approximately 3 $\log_{10}$ increase in intracellular and extracellular viral genome copy numbers at 7 days compared with 1 h post-inoculation (Fig. 2b,c). Accordingly, the infectious titre of secreted viruses was dramatically increased from 1 h (2.4 $\log_{10}$ PFU ml^{-1}) to 7 days (5 $\log_{10}$ PFU ml^{-1}) (Fig. 2d), and this robust increase was also observed in organoids (Extended Data Fig. 1b). Whole-mount immunostaining of entire skin organoids infected for 7 days with MPXV illustrates the extensive presence of viral dsRNA on KRT5-positive regions (Fig. 2e,f). This is further highlighted by zooming into such a region and looking at a single plane of the imaged stack where we observed viral dsRNA in individual KRT5-positive cells (Fig. 2g). The same can also be observed by performing immunostainings on cryosections of infected skin organoids (Fig. 2h). TEM analysis was performed at 7 days after virus inoculation, and the abundant presence of MPXV virions was observed in basal keratinocytes of the skin organoids, which can be distinguished by the presence of specific features such as the basement membrane and hemidesmosomes (Fig. 2i).

End-stage skin organoids that display completely formed hair-bearing follicles were obtained after 130 days in culture[16] (Fig. 3a). After inoculation with MPXV, we observed robust virus replication in organoids (3 $\log_{10}$ increase) and secretion into medium (2 $\log_{10}$ increase), by quantifying viral DNA in organoids and medium from 1 h to 7 days (Fig. 3b,c) respectively. Correspondingly, approximately 2 $\log_{10}$ increase in infectious viral titres in culture medium was observed by plaque assay (Fig. 3d). Robust infections in epithelial surfaces were visualized by co-staining MPXV virions and integrin β4 subunit in skin organoid whole mounts (maximal intensity projections and zoomed-in single *z* plane images, respectively) (Fig. 3e,f). Similar to the replication cycle of vaccinia virus, MPXV is assumed to have four intracellular assembling stages that can be visualized by TEM, initializing from crescent, followed by immature virions and mature virions, and then wrapping by Golgi or endosomal compartment (wrapped virions)[17]. Importantly, we have captured these four successive stages of MPXV virions by TEM analysis (Fig. 3g), and further observed the presence of MPXV virions in keratinocytes (Fig. 3h). These robust infections caused alterations of cell morphology, which appeared to be advanced cell degradation (Extended Data Fig. 2a,b). These results collectively demonstrate that human skin organoids can efficiently support the productive infection of MPXV.

Transcriptomic analyses reveal active MPXV–host interactions

As a large DNA virus, MPXV is estimated to transcribe hundreds of viral genes[18]. We performed transcriptomic analysis on 90-day-old skin organoids infected with MPXV, and revealed a number of abundantly expressed transcripts mapped to the different locations of the MPXV reference genome at day 7 but not 1 h after inoculation (Fig. 4a). A heat map was further generated to display the relative abundance of different viral transcripts. Overall, viral genes are hardly expressed at 1 h post-inoculation, but highly expressed at day 7 (Fig. 4b).

Principal component analysis (PCA) revealed the rewiring of the host transcriptome by MPXV infection (Fig. 4c). Gene Ontology analysis identified upregulated pathways that are associated with immune response, autophagy and antiviral response. Interestingly, several skin-related pathways such as skin development and keratinization were significantly downregulated, indicating that the infection perturbed skin homeostasis in the organoids (Fig. 4d and Extended Data Fig. 3). Consistently, volcano plot analysis identified up- and downregulations of representative genes from these pathways (Extended Data Fig. 4a). Gene set enrichment analysis revealed enrichment of transcriptional signatures such as autophagy, apoptosis, necroptosis

https://doi.org/10.1038/s41564-023-01489-6

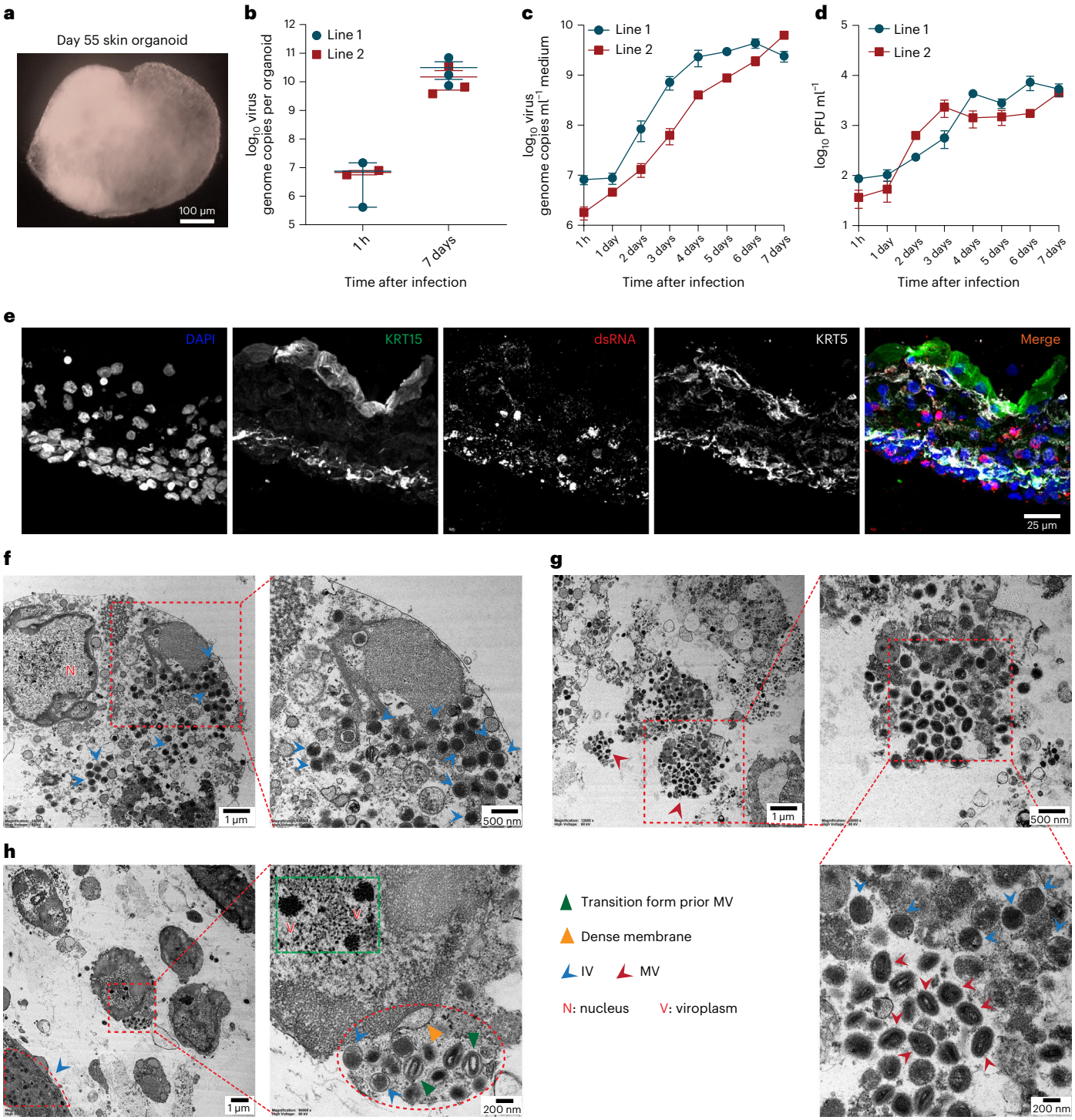

Fig. 1 | MPXV infection in early-stage human skin organoids. a, Bright-field image of human skin organoids at 55 days of differentiation. Scale bar, 100 μm. **b**, Quantification of viral DNA levels in organoids. Each plot represents virus DNA from a single organoid ($n = 4$ for 1 h group, $n = 6$ for 7 days group). **c**, Quantification of viral DNA levels from culture medium (for line 1, $n = 4$ at 1 h post-infection, $n = 3$ at 1 day to 7 days post-infection; for line 2, $n = 5$ at 1 h post-infection, $n = 4$ at 1 day to 7 days post-infection). **d**, Quantification of infectious viral titres of secreted viruses in medium (for line 1, $n = 3$; for line 2, $n = 3$ at 1 h to 3 days post-infection, $n = 4$ at 4 days to 7 days post-infection). **e**, Representative visualization of MPXV-infected organoids by immunostaining with antibodies against KRT5 (white), KRT15 (green), and virus replicating intermediate dsRNA (red), and DAPI nuclei staining (blue). Scale bar, 25 μm. **f**, Representative TEM visualized immature virion (IV) in organoids. Scale bars, 1 μm and 500 nm (magnification). **g**, Representative TEM visualized major mature virion (MV) in organoids. Scale bars, 1 μm, 500 nm and 200 nm (magnification). **h**, TEM visualized intermediate steps of MPXV assembly. Scale bars, 1 μm and 200 nm (magnification). Green frame indicates part of the viral factory containing viroplasm. h, hour post-inoculation; day, day post-inoculation. Data are presented as means of biological replicates ± s.e.m.

https://doi.org/10.1038/s41564-023-01489-6

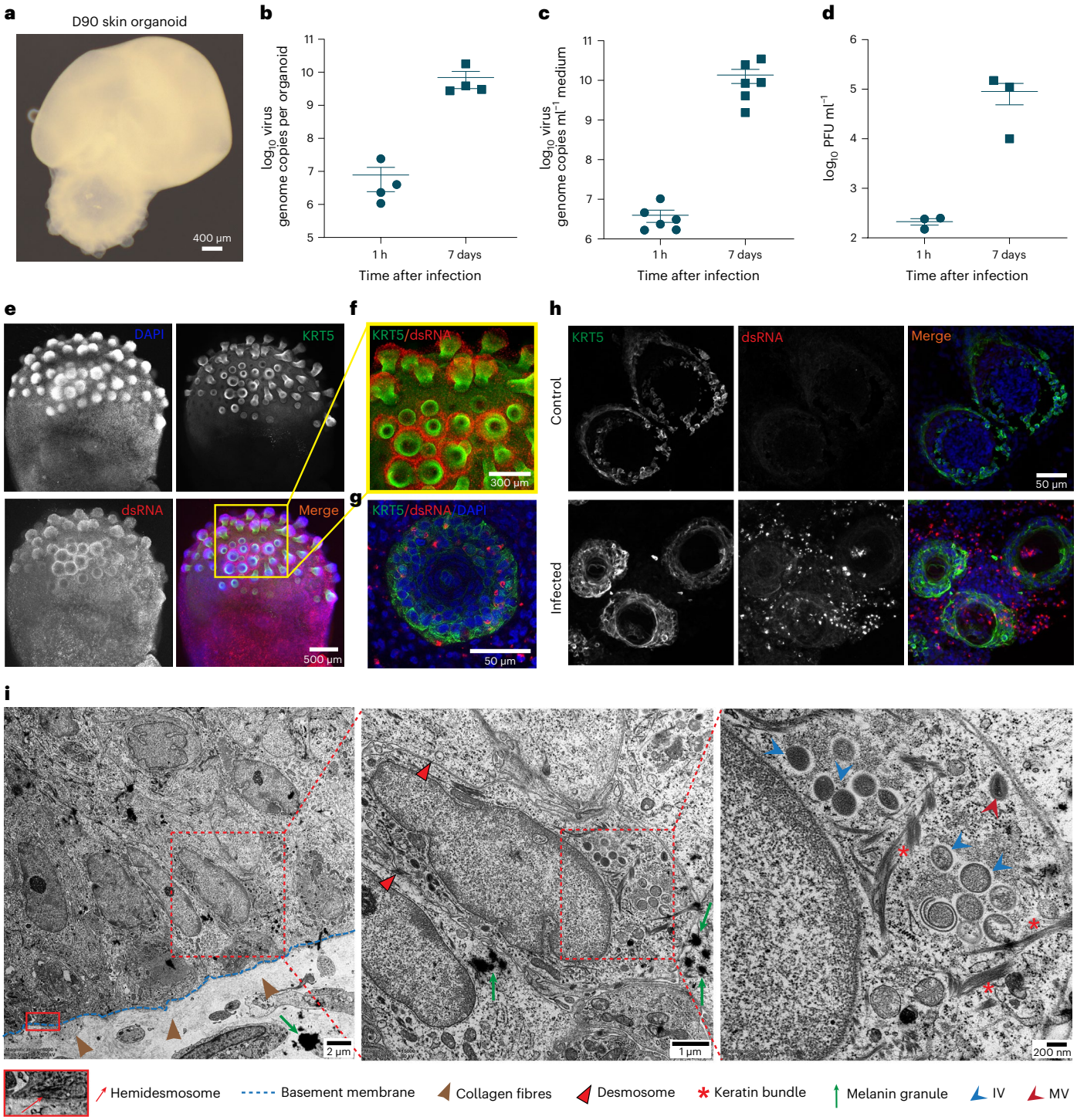

Fig. 2 | MPXV infection in late-stage human skin organoids. a, Bright-field image of human skin organoids at 90 days of differentiation. Scale bar, 400 µm. **b**, Quantification of viral DNA levels in organoids. Each plot represents virus DNA from a single organoid ($n = 4$). **c**, Quantification of viral DNA levels in culture medium. Each plot represents virus DNA from medium of an independent well with a single cultured organoid ($n = 6$). **d**, Quantification of infectious viral titres of secreted viruses in medium ($n = 3$). **e**, Representative visualization of MPXV in keratinocytes by whole-mount staining of KRT5 (green), virus dsRNA (red) and DAPI nuclei staining (blue), by *z*-stack acquisition and projection. Scale bar, 500 µm. **f**, Magnification view of the region in **e** (yellow box). Scale bar, 300 µm. **g**, Representative image of magnification of a region in a single optical plane isolated from the entire *z*-stack showing the presence of dsRNA in individual KRT5-positive cells. Scale bar, 50 µm. **h**, Representative visualization of MPXV in a cryosection by co-staining KRT5 (green) and virus dsRNA (red). Scale bar, 50 µm. **i**, Representative TEM visualized MPXV virions in organoids, in particular keratinocytes. Scale bars, 2 µm, 1 µm and 200 nm. Data are presented as means of biological replicates ± s.e.m.

and ferroptosis in skin organoids of 7 days in comparison with 1 h post-infection (Extended Data Fig. 4b–e).

Analysis of individual genes of interest revealed that important epithelial cell-derived cytokines such as thymic stromal lymphopoietin (TSLP) and interleukin-36 γ (IL36G), which have been implicated in skin pathogenesis[19,20], were upregulated 7 days post-infection (Fig. 4e). More directly, when examining the expression levels of different keratinocyte subpopulation markers, we found that markers of the spinous layer such as keratin 1 (KRT1) and keratin 10 (KRT10) as well as skin barrier-associated genes such as filaggrin (FLG), filaggrin 2 (FLG2), desmoglein 1 (DSG1) and desmocollin 1 (DSC1) were drastically reduced after 7 days of infection (Fig. 4e). Conversely, the expression of basal keratinocyte markers such as integrin α6 (ITGA6), integrin β4 (ITGB4) and keratin 14 (KRT14) was upregulated (Fig. 4e), suggesting that the reduction of spinous layer and skin barrier markers represents a biologically relevant observation. Together these data suggest that MPXV infection causes keratinocyte perturbations and may affect the barrier function of the skin in the organoid model.

Tecovirimat inhibits MPXV in cystic skin organoids

Tecovirimat is a US Food and Drug Administration-approved antiviral drug for treating human smallpox disease. It is currently being explored for treating severe MPXV infection, but the clinical efficacy remains inconclusive. To assess the antiviral activity of tecovirimat in MPXV-infected skin organoids, we first tested a scenario of early antiviral treatment in which tecovirimat was applied 1 h after virus inoculation (Fig. 5a). A range of concentrations, from low (0.1 μM) to clinically relevant blood concentrations (1 μM and 5 μM), were tested. We first quantified the MPXV DNA levels in culture medium at 96 h and 7 days post-inoculation. Significant inhibition was observed at 96 h post-treatment, and the level of inhibition was further increased after 7 days of treatment (Fig. 5b,c). Plaque assay showed potent inhibition of infectious virus production, and plaques were undetectable after 7 days of treatment with 1 or 5 μM of tecovirimat (Fig. 5d). Approximately 2 $\log_{10}$ reduction of intracellular viral DNA was observed in organoids (Fig. 5e). Consistently, a dramatic reduction of MPXV transcripts was observed in tecovirimat-treated skin organoids compared with the untreated organoids at day 7 (40% versus 0.85%) (Fig. 5f and Extended Data Fig. 5). Differential gene expression analysis showed that the impact of rewiring host transcriptome by MPXV infection for 7 days was prevented by tecovirimat treatment (Fig. 5g). This is consistent with the PCA of the host transcriptome showing that the tecovirimat-treated organoids clustered together with the uninfected control (Fig. 4c). At individual gene level, MPXV-triggered induction of epithelial cell-derived cytokines TSLP and IL36G was reduced to basal levels in tecovirimat-treated organoids (Fig. 4e). The inhibitory effects by MPXV infection on markers of the spinous layer (KRT1 and KRT10) and genes associated with skin barrier (FLG, FLG2, DSG1 and DSC1) were prevented by tecovirimat treatment (Fig. 4e).

Next, we tested a scenario of delayed antiviral treatment. We initiated the treatment with 1 μM tecovirimat at 4 days post-infection (Fig. 5h). Quantification of MPXV DNA levels in culture medium showed no inhibition on day 6 to 10 post-infection (corresponding to day 2 to 6 post-treatment), and only minor inhibition on day 12 and 14 post-infection (day 8 to 10 post-treatment, $P = 0.0317$ at day 10 post-treatment) (Fig. 5i). Plaque assay demonstrated very mild inhibition of infectious virus production on day 6 and 8 post-infection (day 2 and 4 post-treatment), and approximately 2 $\log_{10}$ reduction on day 10 post-infection (day 6 post-treatment, $P = 0.0079$), although infectious titres became undetectable on day 12 and 14 post-infection (day 8 and 10 post-treatment) (Fig. 5j). These results collectively suggest that early and late treatments of tecovirimat appear to exert differential effectiveness.

Tecovirimat inhibits MPXV in ALI-cultured skin organoids

Since ALI-cultured skin organoids have recently been shown to better recapitulate structural characteristics of human skin physiology[12], we here tested this method for modelling MPXV infection and testing antiviral treatment (Fig. 6a). After MPXV inoculation on top of the epithelial surface of skin organoids, continuous increase of virus secretion was measured in the medium (dermal side) (over 2 $\log_{10}$ increase of viral genome copies from 1 h to 7 days post-inoculation) (Fig. 6b). Correspondingly, infectious virus titres were undetectable at 1 h but increased up to 3 $\log_{10}$ PFU ml^{-1} at 7 days post-inoculation (Fig. 6c). Next, tecovirimat was administered through the medium to mimic in vivo drug absorption. We observed significant inhibition of virus secretion, with approximately 2 $\log_{10}$ reduction of viral genome copy numbers in medium after 7 days of treatment (Fig. 6b). Importantly, tecovirimat robustly inhibited the production of infectious viruses. No infectious particles were detected in the 7 days treatment group, whereas a viral titre of 3 $\log_{10}$ PFU ml^{-1} viruses was measured in the medium of untreated organoids (Fig. 6d). Consistently, intracellular virus replication was potently inhibited as demonstrated by quantifying viral DNA in organoids after 7 days treatment (Fig. 6e).

Haematoxylin and eosin (H&E) staining and immunostaining indicated that the stratification of ALI-cultured skin organoids closely resembles that of human skin with basal (KRT5), spinous (KRT10) and granular (LOR) markers being expressed. Viral particles were detected in epidermal and dermal layers of infected ALI-cultured skin organoids (Fig. 6f,g and Extended Data Fig. 6). TEM analysis visualized typical skin-associated features, such as keratin bundles, desmosomes and collagen fibres (Extended Data Fig. 2c). Interestingly, we captured the ongoing process of immature virion formation (blue frame in Fig. 6h). Importantly, the four intracellular steps of virion assembly, crescent, immature virions, mature virions and wrapped virions were visualized (Fig. 6i).

Discussion

Human skin organoids exhibit 3D organization of multiple skin cell types with multilayer structures, and are thus considered as the best available in vitro model for studying the physiology and pathology of the skin[16]. Skin organoids have been explored for modelling a variety of diseases including viral infections. Since severe acute respiratory syndrome coronavirus 2 (SARS-CoV-2) can be detected in skin and associated with hair loss in patients[21], human skin organoids have been tested for SARS-CoV-2 infection[13]. Indeed, this model is susceptible to SARS-CoV-2 infection, and can recapitulate the injury to hair follicles and epidermis, resulting in hair loss as seen in patients with coronavirus disease 2019 (ref. 13).

In patients infected with MPXV, skin lesions are the most common symptom[22]. Evidently, MPXV effectively infects and propagates in the

Fig. 3 | MPXV infection in end-stage human skin organoids. a, Bright-field image of skin organoids at 130 days of differentiation. Scale bar, 400 μm. **b**, Quantification of viral DNA levels in organoids. Each plot represents virus DNA from a single organoid ($n = 3$). **c**, Quantification of viral DNA levels in culture medium ($n = 6$). **d**, Quantification of infectious viral titres of secreted viruses in medium ($n = 6$). **e**, Representative images of MPXV in skin organoids by whole-mount immunostaining using an antibody against epithelial marker integrin β4 subunit (red), an antibody against MPXV virions (green), and DAPI nuclei staining (blue). Scale bar, 200 μm. **f**, Representative images of MPXV in single *z* plane optical section of a whole-mounted skin organoid by immunostaining integrin β4 subunit (red) and MPXV (green), and DAPI nuclei staining (blue). Scale bar, 50 μm. **g**, Representative TEM visualized the four intracellular MPXV virions (crescent, immature virion (IV), mature virion (MV) and wrapped virion (WV)) in organoids (black arrowheads show an advanced stage of cell degradation; red frame shows viroplasm forming/entering IV); green frame indicates fibrillar aspect of viral factory. Scale bar, 500 nm. **h**, TEM visualized MPXV virions in keratinocytes. Scale bars, 2 μm, 1 μm and 500 nm. Data are presented as means of biological replicates ± s.e.m.

https://doi.org/10.1038/s41564-023-01489-6

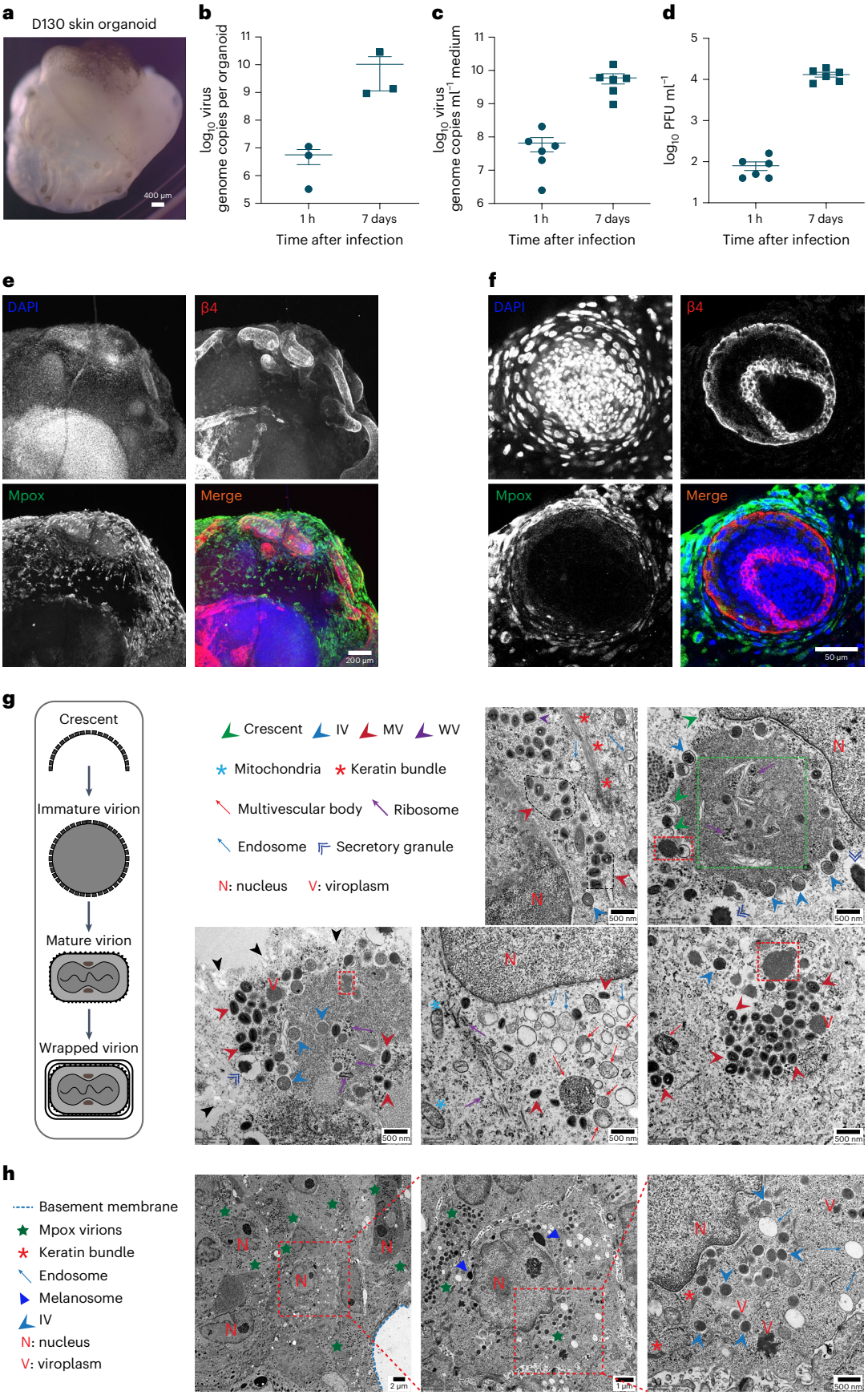

https://doi.org/10.1038/s41564-023-01489-6

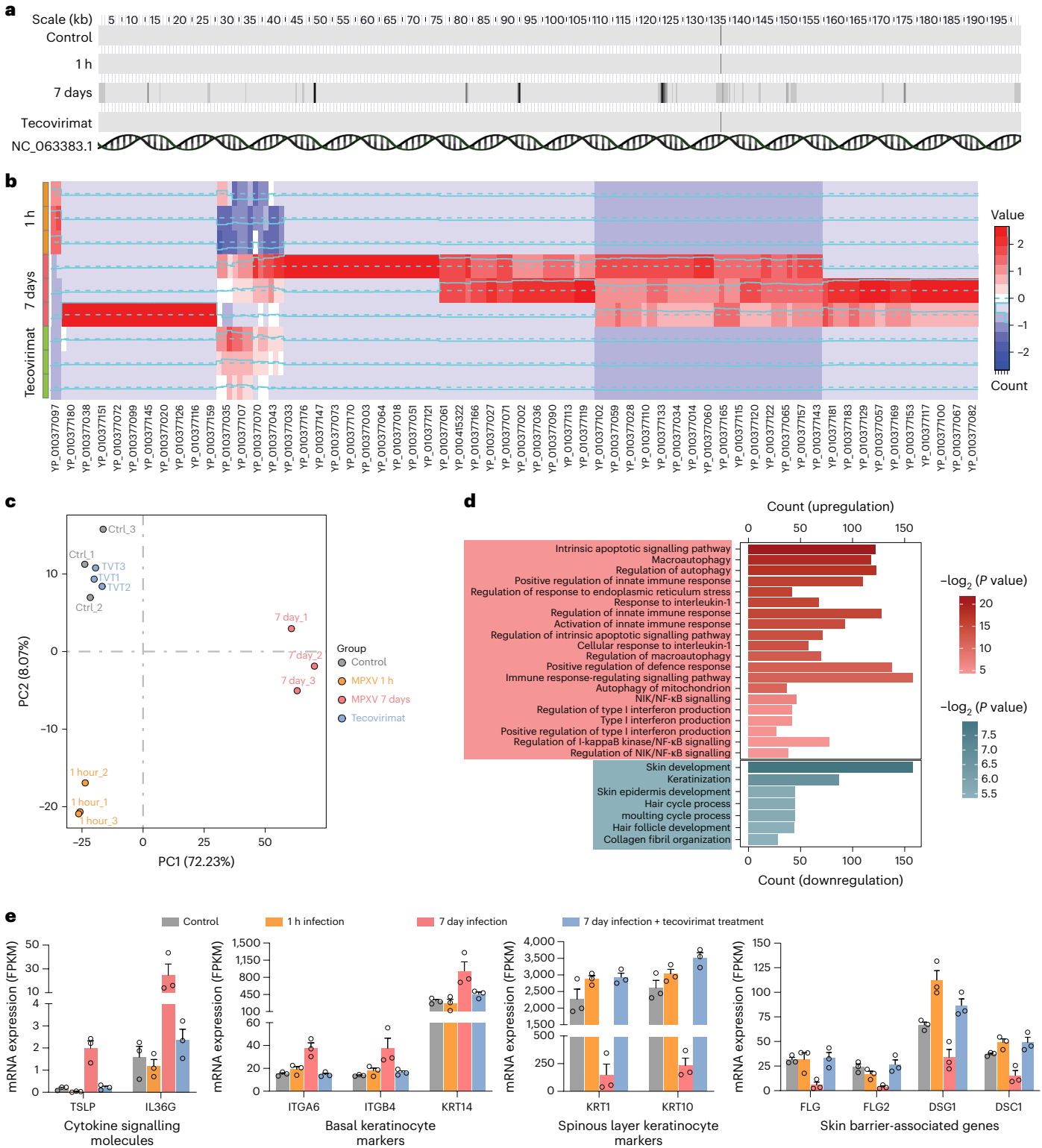

Fig. 4 | Transcriptomic analysis of MPXV-infected organoids. a, MPXV transcripts mapped to the locations in viral genome. **b**, Heat map displaying the expression levels of (putative) viral transcripts at different timepoints and with tecovirimat treatments post-inoculation. *P* value adjusted by Benjamini–Hochberg. **c**, PCA of different groups with three replicates per group (control: uninfected organoids; MPXV-inoculated organoids collected at 1 h and 7 days post-infection; organoids with tecovirimat treatment at 7 days post-infection). **d**, Significantly regulated pathways by Gene Ontology analysis at day 7 post-inoculation, compared with the uninfected group. Red: upregulated; blue: downregulated. *P* value determined by DESeq2. **e**, RNA-sequencing analysis of mRNA expression levels of selected genes associated with skin epithelial cells. Skin organoids were either not infected (control), 1 h post-inoculation (1 h infection), infected for 7 days (7 day infection) or infected and treated with 5 μM of tecovirimat for 7 days (7 days infection + tecovirimat treatment), $n = 3$ for each group. mRNA levels are expressed as fragments per kilobase of transcript per million mapped reads (FKPM). Data are presented as means of biological replicates ± s.e.m.

https://doi.org/10.1038/s41564-023-01489-6

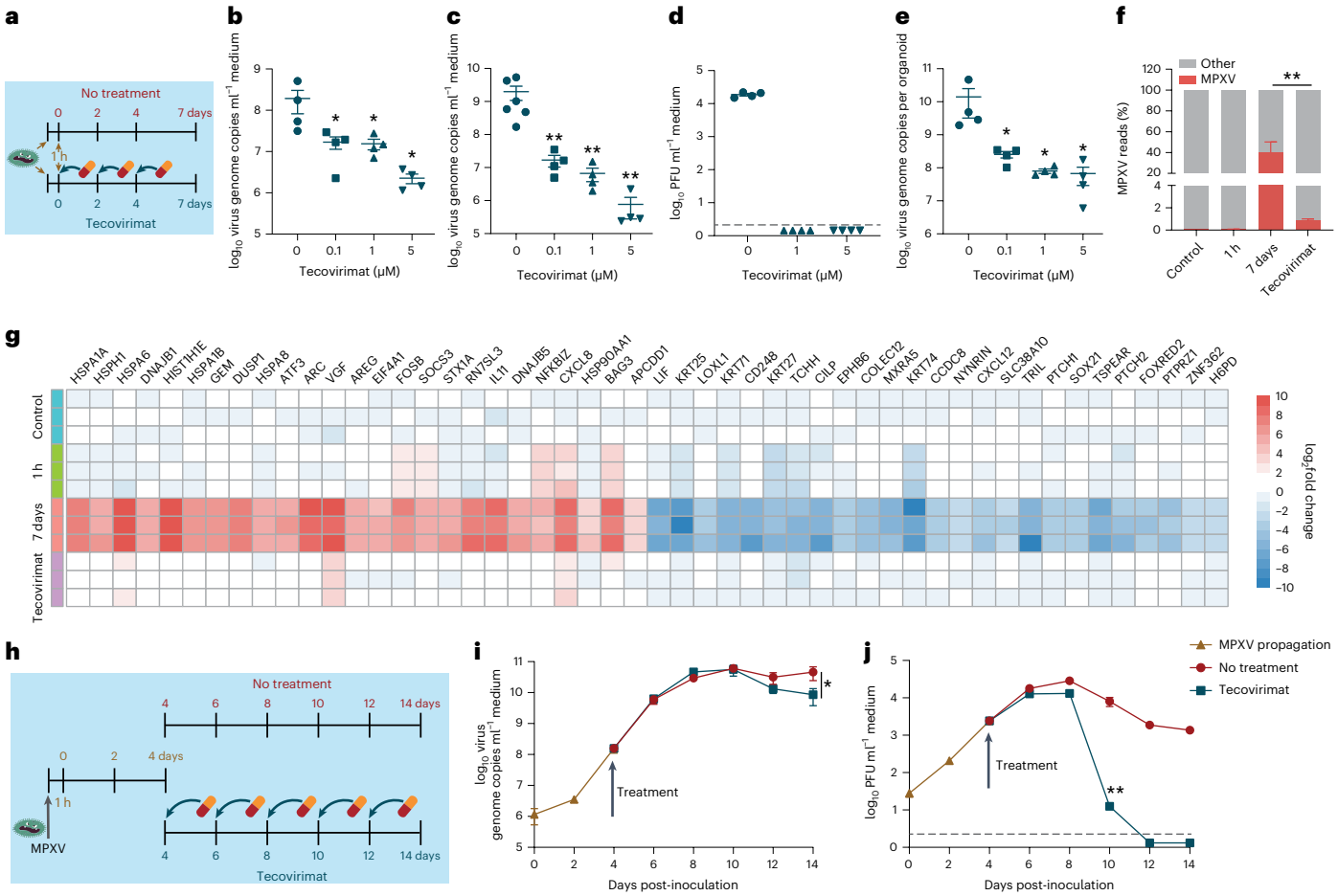

Fig. 5 | MPXV–host interactions and response to tecovirimat treatment. **a**, Schematic representation of early tecovirimat treatment in skin organoids. **b**,**c**, Quantification of MPXV DNA level in culture medium at 96 h (**b**) and 7 days (**c**) after tecovirimat treatment (in **b**, $n = 4$ for each group; in **c**, $n = 6$ for no treatment group, $n = 4$ for tecovirimat group). **d**, Quantification of infectious titres in culture medium at 7 days after tecovirimat treatment. Infectious virus titres were undetectable in the treatment groups ($n = 4$). **e**, Quantification of MPXV DNA level in organoids at 7 days after tecovirimat treatment ($n = 4$). **f**, The percentages of mapped MPXV transcripts in different groups of organoids ($n = 3$, $P < 0.001$). **g**, Top 50 significantly regulated genes upon MPXV infection. **h**, Schematic representation of delayed tecovirimat treatment in skin organoids. **i**,**j**, Quantification of MPXV DNA level (**i**) and infectious titres (**j**) in culture medium at 1 h (0 day), 2 days, 4 days, 6 days, 8 days, 10 days, 12 days and 14 days post-inoculation. Tecovirimat (1 μM) was administered at 4 days post-inoculation. Data are shown as mean ± s.e.m. In **i**, $n = 10$ for MPXV propagation, n = 5 for no treatment and tecovirimat treatment group. In **j**, $n = 5$ for each group. **b**, **c**, **e**, **i** and **j** use Mann–Whitney test with two tailed; **f** uses χ^2 test. $^*P < 0.05$ (for **i**, $P = 0.0317$), $^{**}P < 0.01$ (for **j**, $P = 0.0079$). The dashed line indicates that infectious titres were undetectable. Data are presented as means of biological replicates ± s.e.m.

skin of the infected patients[23]. However, there is a lack of human-derived experimental models to authentically recapitulate this infection. Here we demonstrated that human cystic skin organoids are highly permissive for MPXV infection, with viral genome copies and infectious titres dramatically increasing over time in particular within the first week post-inoculation. Interestingly, the production of infectious viruses gradually decreased in the second week of infection in our skin organoids. This may resemble the self-limiting course of MPXV infection, which in general lasts 2–4 weeks in patients[24].

Next, we took advantage of further technological developments of culturing skin organoids into ALI system[12]. This system shows the advantages of being mainly byproduct free, in a physiological configuration (epidermis up, dermis down) and endowed with hair follicles that are known to play a key role in barrier function of the skin. We confirmed that these keratinocytes support the full lifecycle of MPXV infection. In both model systems, cystic structured and ALI-cultured skin organoids, the four intracellular successive stages of MPXV assembly that have been previously described[17] as well as multiple intermediate steps have been observed in infected cells by TEM. Interestingly, a recent study on vaccinia virus further classified intracellular mature viruses into nascent and mature virions, although these two forms are indistinguishable by TEM[25]. Thus, it would be intriguing to investigate whether these newly classified forms also exist for MPXV.

Genome-wide transcriptome analysis revealed profound rewiring of host gene transcription by active MPXV infection, whereas tecovirimat treatment largely impeded this process. Gene Ontology analysis indicates that several pathways associated with skin and hair development are significantly downregulated. This is in line with the fact that MPXV infection is particularly pathogenic to skin tissues. Furthermore, we identified transcriptional signatures associated with apoptosis, necroptosis and ferroptosis, which may explain the underlying mechanism of skin injury in patients. When interrogating our datasets for the expression levels of individual genes of interest, we observed specific effects of MPXV infection on keratinocytes of the skin organoids through induction of epithelial-derived cytokines such as TSLP and IL36G and the downregulation of skin barrier-associated genes. TSLP is known to be involved in skin conditions such as atopic dermatitis[19], and was also recently found to be induced in *Staphylococcus aureus*-infected skin organoids in ALI culture[12]. IL36G expression was found to be highly induced in human keratinocytes by adding dsRNA

https://doi.org/10.1038/s41564-023-01489-6

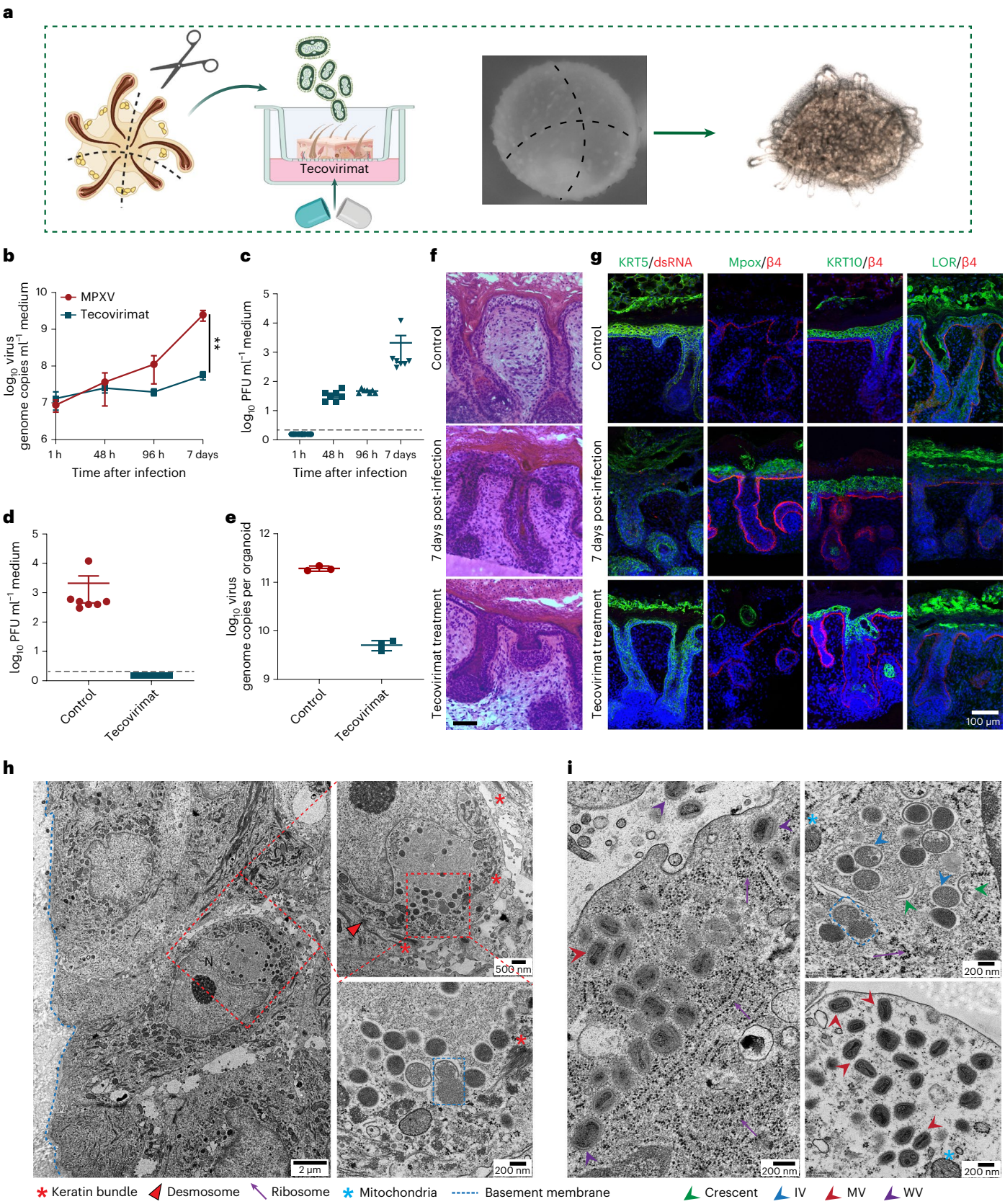

analogue polyinosinic-polycytidylic acid, raising the possibility that viral dsRNA may have a similar effect in our skin organoid model[20]. Furthermore, we found that MPXV infection is associated with the downregulation of genes specifically associated with the skin barrier, a feature that requires complex model systems to be captured.

Efficient propagation of MPXV in skin organoids inevitably requires exploitation of host metabolic machineries, which is supported by our observation that multiple catabolism- and metabolism-related pathways are dysregulated. Our previous studies of modelling infections of different RNA viruses in human intestinal, liver and lung organoids

Fig. 6 | MPXV infection and antiviral treatment in skin organoids cultured in ALI. a, Schematic diagram for MPXV infection and treatment in organoids cultured in ALI. **b**, Quantification of MPXV DNA level in culture medium from organoids with tecovirimat treatment or without treatment ($n = 6$, $P = 0.0286$). **c**, Kinetics of infectious viral titres in the culture medium from 1 h to 7 days post-inoculation ($n = 7$). **d**, Quantification of infectious virus titres in culture medium at 7 days after tecovirimat treatment. Infectious virus titres were undetectable in the treatment group ($n = 7$). **e**, Quantification of viral DNA level in skin organoids at 7 days after tecovirimat treatment ($n = 3$). **f**, Representative bright-field images of ALI-skin organoids stained with H&E. Scale bar, 50 µm. **g**, Representative immunostaining with antibodies against epithelial layer markers KRT5 (basal layer), KRT10 (spinous layer) and LOR (granular layer) as well as against MPXV virion, virus replicating dsRNA or integrin β4 subunit. Scale bar, 100 µm. **h**, Representative TEM images visualized skin-associated landmarks and MPXV virions (blue frame shows the process of forming immature virion). Scale bars, 2 µm, 500 nm and 200 nm (magnification). **i**, Representative TEM images visualized different MPXV virions in ALI-skin organoids. Scale bar, 200 nm. Data are shown as means of biological replicates ± s.e.m, $^{**}P < 0.01$, Mann–Whitney test, two tailed. IV, immature virion; MV, mature virion; WV, wrapped virion.

ubiquitously activated robust antiviral interferon response with the induction of a large set of interferon-stimulated genes[26–28]. In contrast, the activation of this classical antiviral response was minimal in MPXV-infected skin organoids. In line with our findings, previous evidence indicates that orthopoxviruses are capable of antagonizing cytosolic DNA sensing and antiviral response, thereby effectively evading host innate immunity[29,30].

Two antiviral drugs, brincidofovir and tecovirimat, have been approved for treating smallpox, and are effective in inhibiting MPXV infection in experimental models. Tecovirimat inhibits orthopoxvirus by disrupting a major envelope wrapping protein VP37 and is more potent than brincidofovir as shown in experimental models[31]. In this specific case, the US Food and Drug Administration approval of tecovirimat for treating smallpox was based on well-controlled animal studies using related orthopoxviruses including MPXV[32], but efficacy demonstrated in animals does not always translate into efficacy in patients[33]. Nevertheless, given the urgent clinical need and an acceptable safety profile in tested healthy individuals, tecovirimat is increasingly being prescribed for compassionate use for treating MPXV infection[34]. In cultured Vero cells, tecovirimat has been shown to be highly efficacious against a MPXV isolate from the 2022 outbreak even at nanomolar concentrations[35]. In treated patients, achievable blood concentrations of tecovirimat range from 1 to 5 µM (ref. 36), but the effect on MPXV viral load remains inconclusive[37]. In mice infected with a 2022 MPXV isolate, treatment of tecovirimat resulted in about 2 $\log_{10}$ reduction of viral titres on day 7 in lung tissues[38]. In our skin organoids, tecovirimat was initially applied immediately after virus inoculation. Tecovirimat treatment ranging from 0.1 to 5 µM for 7 days resulted in 2 to 3 $\log_{10}$ reduction in viral DNA load. Importantly, no infectious virus was detected in culture medium after 7 days treatment.

In clinical practice, it is common to have a delay in prescribing antiviral treatment for mpox patients. A large clinical study investigating tecovirimat treatment for 549 patients with mpox from the United States, May to August 2022, reported that the median time between the onset of symptoms and the first dosage of tecovirimat was 7 days (ref. 39). In another study reporting three fatal cases of mpox in people with uncontrolled human immunodeficiency virus, all patients received tecovirimat treatment 14 days after disease onset at the earliest, mainly because of inability to access the medication initially[40]. To test a delayed antiviral treatment scenario, we first infected skin organoids with MPXV for 4 days, and then treated with tecovirimat at 1 µM for the subsequent 10 days. We observed minimal effects on viral DNA load in the culture medium. The inhibition on production of infectious viruses was also very mild during the first 4 days of treatment, which was more apparent on day 6 and eventually became undetectable on days 8 and 10 of treatment. The disparities in viral DNA and infectious titre reduction in both experimental schemes are consistent with the mechanism-of-action of tecovirimat that prevents the production of infectious poxviruses[32]. Although tecovirimat is being widely prescribed, it remains inconclusive regarding the effectiveness for treating mpox, because proper control groups are usually not available for comparison[39,41]. Our results of delayed tecovirimat treatment in skin organoids compromising the effectiveness highlight the importance of early initiation of the treatment for infected patients, which is in fact a major challenge in clinical practice. Mechanistically, future studies should better characterize the impact of tecovirimat on the different stages of MPXV biogenesis in experimental models, and if possible in biopsies from treated patients.

Notably, a number of animal models have been developed for MPXV infection, but it remains unclear how faithfully these models recapitulate the infection and disease in humans, in particular the lacking of skin manifestations[42]. The availability of human in vitro models is essential for in-depth studies to the pathogenic mechanisms of MPXV and for discovering therapeutics. Currently available in vitro models are exclusively based on immortalized cell lines[43]. These cell lines have many epigenetic, genetic and functional alterations that fail to adequately model many aspects of human diseases[27] and lack interactions between different cell types present in tissues. Here we show that human skin organoids in cystic structure or ALI culture can authentically recapitulate virus–host interactions and evaluate antiviral drug efficacy. This system, standalone or in combination with conventional models, could serve as an innovative tool for MPXV research. Nevertheless, the pathogenesis of MPXV infection such as pathological inflammation also involves immune cells, which are currently lacking in our skin organoids. Future improvement, for example by incorporating the relevant immune cell populations, would further advance this system for better disease modelling and therapeutic development.

In summary, human skin organoids support the productive infection of MPXV and recapitulate active virus–host interactions. Tecovirimat treatment inhibited MPXV infection in this model. Our findings shall help to better understand the pathogenesis of MPXV-induced skin injury, and facilitate future research into MPXV–host interactions and antiviral drug development.

Methods

Skin organoid generation

Three previously described hiPS cell lines (LUMCi004-A, LUMCi031-A and WT2) were used to generate skin organoids (hpscreg.eu)[44]. Lines were maintained in an undifferentiated state as described[15]. Hair-bearing skin organoids were generated as previously described[11,15]. In short, the hiPS cell lines were cultured in StemFlex medium (SFM, Thermo Fisher Scientific) on vitronectin-coated plates (STEMCELL Technologies) and passaged twice a week as single cells by using Gentle Cell Dissociation Reagent (STEMCELL Technologies) at a density of 2.5×10^4 cells cm^{-2}. Incubation was performed in a 37 °C incubator with 5% CO_2. For hair-bearing skin organoids generation, cells were dissociated by using Gentle Cell Dissociation Reagent and 3,500 cells in 100 µl of SFM containing 10 µM Y27632 (Bio-Connect) were dispensed into 96 wells of a U-bottom low-attachment plate (Thermo Scientific), spun down (110 r.c.f., 6 min) and incubated for 24 h. A volume of 100 µl of SFM was then added, and 24 h later (day 0 of differentiation) aggregates were washed three times in 1 ml of Essential 6 medium (E6M, Gibco) and transferred to new 96 wells of a U-bottom plate in 100 µl of E6M containing 2% Matrigel (Corning), 10 µM SB431542 (R&D Systems), 4 ng ml^{-1} fibroblast growth factor (Tebubio), 2.5 ng ml^{-1} BMP4 (R&D Systems) and 100 µg ml^{-1} Normocin (Invivogen). Three days later, 25 µl of E6M containing 1 µM LDN 193189 (Bio-Techne), 250 ng ml^{-1} fibroblast growth factor and 100 µg ml^{-1} Normocin was added. Three days later,

75 µL of E6M containing 100 µg ml^{-1} Normocin was added. Two and 4 days later, 100 µl of medium was carefully removed and refreshed by 100 µl of E6M containing 100 µg ml^{-1} Normocin. Two days later, aggregates were washed three times in 1 ml of advanced Dulbecco's modified Eagle medium (DMEM)/F12 medium (Gibco), and each aggregate was transferred to a well of a low-attachment 24-well plate (Thermo Scientific) in 500 µl of Organoid Maturation Medium (OMM, composed of 49% advanced DMEM/F12, 49% Neurobasal medium (Gibco), 1× GlutaMAX (Gibco), 0.5× B2-27 minus vitamin A (Gibco), 0.5× N-2 (Gibco), 0.1 mM 2-mercaptoethanol (Gibco) and 100 µg ml^{-1} Normocin) containing 1% Matrigel (OMM1%M). Three days later, 250 µl of medium was carefully removed and replaced by 250 µl OMM1%M. Two days later (day 18 of differentiation), 250 µl of medium was removed and replaced by 250 µl OMM (without Matrigel). From day 18 to 45, half medium change was performed every 3 days using OMM. From day 45 onwards, half medium change was performed every other day, including full medium change once a week. From day 80 onwards, the volume of OMM was increased to 1 ml.

ALI skin organoid culture

Cyst-like skin organoids at days 75–90 of differentiation were cut into four and placed epidermis-up on type I-collagen-coated Transwell culture insert (2 mg ml^{-1}) placed on a 12-well plate containing 600 µl of OMM[12]. After 3 weeks of ALI culture in a humidified incubator at 37 °C with 5% CO_2, ALI-skin organoids were transferred for 6 days to an incubator without humidity at 37 °C with 5% CO_2 (dry conditions). OMM was replaced every 2 days when cultured in humidified conditions and daily when cultured in dry conditions. Schematic representation was illustrated with BioRender.

MPXV infection and antiviral treatment

Cell culture-propagated MPXV virus particles originating from a patient isolate of the 2022 outbreak were used in this study (European Virus Archive, Ref-SKU: 010V-04721). Three representative stages of skin organoids were used to inoculate with MPXV, namely the early stage of 55 days of differentiation (hair germs formed), the late stage of 90 days of differentiation (more hair germ and hair pegs formed) and the end stage of 130 days of differentiation (hair follicles formed). Individual skin organoids of all stages were inoculated with approximately 10^5 PFU MPXV and incubated at 37 °C for 2 h. After 2 h incubation, viral inoculum was removed, and organoids were washed three times by phosphate-buffered saline (PBS). Skin organoids were then cultured in 24-well plate supplemented with 500 µl culture medium per well. Culture medium was collected and/or organoids were lysed at 1 h, 48 h, 96 h and 7 days post-inoculation for future DNA isolation. For skin organoids cultured in ALI, 10^5 PFU virus was inoculated on the top of the epithelial surface of each organoid, and incubated at 37 °C for 2 h. After incubation, virus inoculum was removed and gently washed twice with PBS. Culture medium (600 µl per well of 24-well plate) was then added to the bottom of the well so that it comes in contact with the dermal side of the organoid while the insert and epithelial surface of the organoid remain dry. For early treatment of antiviral drug, skin organoids were first inoculated with MPXV for 2 h, and culture medium containing serial concentrations of tecovirimat (Selleckchem) was supplemented immediately after inoculation. Medium was refreshed on day 2 and day 4 post-infection. In addition, delayed antiviral treatment was tested by administering 1 µM of tecovirimat to end-stage organoids at 4 days post-infection. Culture medium was collected at 1 h (0 day), 2 days, 4 days, 6 days, 8 days, 10 days, 12 days and 14 days post-inoculation for DNA isolation and plaque assay.

DNA extraction and qPCR detection

Total DNA was purified from infected organoids or culture medium using Macherey-Nagel NucleoSpin DNA Kit (BIOKÉ) and quantified by Nanodrop ND-1000. Viral DNA levels were quantified by SYBR Green-based qRT–PCR (Applied Biosystems SYBR Green PCR Master Mix; Thermo Fisher Scientific Life Sciences) with the StepOnePlus System v2.3 (Thermo Fisher Scientific Life Sciences). MPXV viral DNA was detected by primers 'Forward- GGCTCTTCTATCAACCACA; Reverse-AGTCATTATCTCCTCCTCCA', and calculated by previously generated formula '$y = -0.3095x + 15.387$'.

Plaque assay

Skin organoids were collected and stored in 1 ml serum-free advanced DMEM/F12 medium (with 1× GlutaMAX, 1 M HEPES and 1% penicillin/streptomycin), and centrifuged after three cycles of freezing and thawing to collect clear cell lysates as intracellular viruses. Cleared supernatants from culture medium were used as extracellular viruses. Confluent Vero cells in 12-well plates were washed once with PBS before virus inoculation. Next, Vero cells were overlaid with 1.2% avicel in serum-free advanced DMEM/F12 medium (with 1× GlutaMAX, 1 M HEPES and 1% penicillin/streptomycin) containing ten-fold serial dilutions of samples. Plates were incubated 3 days at 37 °C and then fixed by 4% paraformaldehyde (PFA) and stained with 0.1% crystal violet. Plaques were quantified as PFU ml^{-1}. Data were presented as the common logarithm, and the samples with undetectable plaque were arbitrarily denoted with a value '1'.

Embedding of ALI-cultured organoids

ALI-cultured organoids were fixed in 0.2 % (w/v) PFA in 0.1 M phosphate buffer (PB) containing 0.12 mM $CaCl_2$ and 4% (w/v) sucrose (solution I, pH 7.4) for 16 h at 4 °C. They were washed in solution I for 12 h at 4 °C and then in PB containing 15% (w/v) sucrose for 16 h at 4 °C. Organoids were then incubated in PB with 15% sucrose and 7.5% gelatin for 1 h at 37 °C, immediately frozen in liquid nitrogen-chilled isopentane, and stored at 80 °C until sectioned[45].

Histology

Cryosections of ALI-cultured skin organoids were stained with H&E. Images were acquired with an Olympus AX70 microscope using an Olympus XC50 digital colour camera.

Immunofluorescence staining and image acquisition

For cryosections, entire organoids were embedded in Tissue-Tek O.C.T. compound (Sakura, catalogue no. 4583) embedding matrix. Sections (10 µm thick) were fixed for 10 min in ice-cold acetone and blocked with 2% bovine serum albumin (BSA; Sigma) in PBS for 1 h at room temperature (RT). Incubations with primary and secondary antibodies were performed in PBS 2% BSA for 1 h at RT (details of the antibodies used and concentrations are provided in Supplementary Information). Nuclei were stained with 4′,6-diamidino-2-phenylindole (DAPI). Sections were mounted in Fluoromount-G (SouthernBiotech). For whole-mount immunostaining, organoids were fixed in 4% PFA for 16 h at 4 °C and incubated in Scale S0 (pH 7.2) composed of 20% (w/v) D-(−)-sorbitol, 5% glycerol, 1 mM methyl-β-cyclodextrin, 1% (w/v) *N*-acetyl-L-hydroxyproline, 3% dimethyl sulfoxide in 1× Dulbecco's PBS, no calcium, no magnesium (DPBS, ThermoFisher Scientific, catalogue no. 14190144) for 8 h at 37 °C. They were permeabilized by successive incubations in Scale A2 (pH 7.7) composed of 10% glycerol, 4 M urea and 0.1% Triton X-100 in de-ionized H_2O for 36 h at 37 °C; in Scale B4(0) (pH 8.4) composed of 8 M urea for 24 h at 37 °C and in Scale A2 for 12 h at 37 °C. Skin organoids were incubated in DPBS for 6 h at RT, and primary antibodies were incubated in AbScale solution composed of 0.33 M urea, 0.1% Triton X-100 in DPBS for 36 h at 37 °C. After two washing steps in AbScale solution for 2 h at RT, secondary antibodies were incubated in AbScale solution for 36 h at 37 °C and washed in AbScale solution for 6 h at RT two times in AbScale Rinse solution composed of 0.1% DPBS containing 2.5% BSA and 0.05% Tween 20, for 2 h at RT. After refixation in 4% PFA for 1 h at RT, skin organoids were washed 1 h in DPBS containing DAPI for 1 h at RT and cleared in Scale S4 (pH

7.9) composed of 40% (w/v) D-(−)-sorbitol, 10% glycerol, 4 M urea and 15% (v/v) dimethyl sulfoxide for 16 h at 37 °C. They were mounted and imaged in Scale S4 (ref. 11). Microscopy images were acquired with a Zeiss LSM900 Airyscan2 upright confocal microscope, or with a Leica TCS SP5 confocal microscope.

Genome-wide RNA sequencing and data analysis

Four groups of organoids were prepared for bulk RNA sequencing: skin organoids cultured for 1 h post-inoculation; skin organoids cultured for 7 days post-inoculation; skin organoids treated with 5 µM tecovirimat post-inoculation; skin organoids without virus infection were cultured in the same conditions for 7 days and were used as non-infected controls. Finally, three samples per condition were processed to extract total RNA following the Macherey-Nagel NucleoSpin RNA II Kit (BIOKÉ). Extracted RNA was first measured by Bioanalyzer RNA 6000 Picochip, followed by RNA sequencing performed by Novogene with paired-end 150 bp (PE 150) sequencing strategy. For viral gene mapping, raw reads from every dataset were quality controlled using fastp[46] with average quality parameter set to 30. These quality control reads were then mapped using Burrows-Wheeler Transform aligner[47] to mpox genome (accession NC_063383.1, assembly GCF_014621545.1). This version of mpox genome is also available on UCSC Genome Browser (UCSC Genome Brower Instance with mpox genome[48]). Read mapping rates were calculated using samtools[49]. Read counts were used for differential expression analyses. For differential expression analysis of MPXV transcripts, the R 'edgeR' was used with Benjamini–Hochberg for *P*-value adjustment and 10^{-5} as threshold for the false discovery rate. The clustering was made by using the Euclidean distance and R 'hclust' function as clustering function.

See additional materials and reagents in Supplementary Information.

Statistics and reproducibility

All statistical analyses were completed using GraphPad Prism 8.0 or R software. Comparison between two groups was analysed by Mann–Whitney *U* test. Data are presented as mean ± standard error of the mean (s.e.m.). $P < 0.05$ was considered statistically significant. For immunofluorescence staining and electron microscopy, at least two biological replicates were prepared, and representative images were selected in the manuscript.

Reporting summary

Further information on research design is available in the Nature Portfolio Reporting Summary linked to this article.

Data availability

The data supporting the findings of this study are available within the paper, its supplementary information or its source data. RNA sequencing data are publicly available at https://doi.org/10.17026/dans-xj2-hhat. Mpox viral reads were mapped according to the reference genome (accession NC_063383.1). Source data are provided with this paper.

Code availability

The code used for transcriptomics analysis in this study is publicly available at https://doi.org/10.17026/dans-xzc-46u4

References

1. Gessain, A., Nakoune, E. & Yazdanpanah, Y. Monkeypox. *N. Engl. J. Med.* **387**, 1783–1793 (2022).
2. Lum, F. M. et al. Monkeypox: disease epidemiology, host immunity and clinical interventions. *Nat. Rev. Immunol.* **22**, 597–613 (2022).
3. Thornhill, J. P. et al. Monkeypox virus infection in humans across 16 Countries—April–June 2022. *N. Engl. J. Med.* **387**, 679–691 (2022).
4. Zheng, Q. et al. Projecting the impact of testing and vaccination on the transmission dynamics of the 2022 monkeypox outbreak in the USA. *J. Travel Med.* **29**, taac101 (2022).
5. McCollum, A. M. & Damon, I. K. Human monkeypox. *Clin. Infect. Dis.* **58**, 260–267 (2014).
6. Adler, H. et al. Clinical features and management of human monkeypox: a retrospective observational study in the UK. *Lancet Infect. Dis.* **22**, 1153–1162 (2022).
7. Girometti, N. et al. Demographic and clinical characteristics of confirmed human monkeypox virus cases in individuals attending a sexual health centre in London, UK: an observational analysis. *Lancet Infect. Dis.* **22**, 1321–1328 (2022).
8. Ogoina, D. et al. Clinical course and outcome of human monkeypox in Nigeria. *Clin. Infect. Dis.* **71**, e210–e214 (2020).
9. Boesecke, C., Monin, M. B., van Bremen, K., Schlabe, S. & Hoffmann, C. Severe monkeypox-virus infection in undiagnosed advanced HIV infection. *Infection* **50**, 1633–1634 (2022).
10. Rosa, R. B. et al. In vitro and in vivo models for monkeypox. *iScience* **26**, 105702 (2023).
11. Lee, J. et al. Hair-bearing human skin generated entirely from pluripotent stem cells. *Nature* **582**, 399–404 (2020).
12. Jung, S. Y. et al. Wnt-activating human skin organoid model of atopic dermatitis induced by *Staphylococcus aureus* and its protective effects by *Cutibacterium acnes*. *iScience* **25**, 105150 (2022).
13. Ma, J. et al. Establishment of human pluripotent stem cell-derived skin organoids enabled pathophysiological model of SARS-CoV-2 infection. *Adv. Sci.* **9**, e2104192 (2022).
14. Ma, J. et al. Application of an iPSC-derived organoid model for localized scleroderma therapy. *Adv. Sci.* **9**, e2106075 (2022).
15. Ramovs, V. et al. Characterization of the epidermal-dermal junction in hiPSC-derived skin organoids. *Stem Cell Rep.* **17**, 1279–1288 (2022).
16. Lee, J. et al. Generation and characterization of hair-bearing skin organoids from human pluripotent stem cells. *Nat. Protoc.* **17**, 1266–1305 (2022).
17. Weisberg, A. S. et al. Enigmatic origin of the poxvirus membrane from the endoplasmic reticulum shown by 3D imaging of vaccinia virus assembly mutants. *Proc. Natl Acad. Sci. USA* **114**, E11001–E11009 (2017).
18. Yang, Z., Bruno, D. P., Martens, C. A., Porcella, S. F. & Moss, B. Simultaneous high-resolution analysis of vaccinia virus and host cell transcriptomes by deep RNA sequencing. *Proc. Natl Acad. Sci. USA* **107**, 11513–11518 (2010).
19. Wilson, S. R. et al. The epithelial cell-derived atopic dermatitis cytokine TSLP activates neurons to induce itch. *Cell* **155**, 285–295 (2013).
20. Lian, L. H., Milora, K. A., Manupipatpong, K. K. & Jensen, L. E. The double-stranded RNA analogue polyinosinic-polycytidylic acid induces keratinocyte pyroptosis and release of IL-36γ. *J. Invest. Dermatol.* **132**, 1346–1353 (2012).
21. Subramanian, A. et al. Symptoms and risk factors for long COVID in non-hospitalized adults. *Nat. Med.* **28**, 1706–1714 (2022).
22. Altindis, M., Puca, E. & Shapo, L. Diagnosis of monkeypox virus—an overview. *Travel Med. Infect. Dis.* **50**, 102459 (2022).
23. Suner, C., et al. Viral dynamics in patients with monkeypox infection: a prospective cohort study in Spain. *Lancet Infect. Dis.* **23**, 445–453 (2022).
24. Gupta, A. K., Talukder, M., Rosen, T. & Piguet, V. Differential diagnosis, prevention, and treatment of mpox (Monkeypox): a review for dermatologists. *Am. J. Clin. Dermatol.* **24**, 541–556 (2023).
25. Holley, J. et al. Engineered promoter-switched viruses reveal the role of poxvirus maturation protein A26 as a negative regulator of viral spread. *J. Virol.* **95**, e0101221 (2021).

26. Li, P. et al. Recapitulating infection, thermal sensitivity and antiviral treatment of seasonal coronaviruses in human airway organoids. *EBioMedicine* **81**, 104132 (2022).
27. Li, P. et al. Recapitulating hepatitis E virus–host interactions and facilitating antiviral drug discovery in human liver-derived organoids. *Sci. Adv.* **8**, eabj5908 (2022).
28. Yin, Y. et al. Modeling rotavirus infection and antiviral therapy using primary intestinal organoids. *Antivir. Res* **123**, 120–131 (2015).
29. El-Jesr, M., Teir, M. & Maluquer de Motes, C. Vaccinia virus activation and antagonism of cytosolic DNA sensing. *Front. Immunol.* **11**, 568412 (2020).
30. Albarnaz, J. D. et al. Molecular mimicry of NF-κB by vaccinia virus protein enables selective inhibition of antiviral responses. *Nat. Microbiol.* **7**, 154–168 (2022).
31. Yang, G. et al. An orally bioavailable antipoxvirus compound (ST-246) inhibits extracellular virus formation and protects mice from lethal orthopoxvirus challenge. *J. Virol.* **79**, 13139–13149 (2005).
32. Grosenbach, D. W. et al. Oral tecovirimat for the treatment of smallpox. *N. Engl. J. Med.* **379**, 44–53 (2018).
33. Sherwat, A., Brooks, J. T., Birnkrant, D. & Kim, P. Tecovirimat and the treatment of monkeypox—past, present, and future considerations. *N. Engl. J. Med.* **387**, 579–581 (2022).
34. Desai, A. N. et al. Compassionate use of tecovirimat for the treatment of monkeypox infection. *JAMA* **328**, 1348–1350 (2022).
35. Frenois-Veyrat, G. et al. Tecovirimat is effective against human monkeypox virus in vitro at nanomolar concentrations. *Nat. Microbiol* **7**, 1951–1955 (2022).
36. Chinsangaram, J. et al. Pharmacokinetic comparison of a single oral dose of polymorph form i versus form V capsules of the antiorthopoxvirus compound ST-246 in human volunteers. *Antimicrob. Agents Chemother.* **56**, 3582–3586 (2012).
37. Mondi, A. et al. Clinical experience with use of oral tecovirimat or intravenous cidofovir for the treatment of monkeypox in an Italian reference hospital. *J. Infect.* **86**, 66–117 (2023).
38. Warner, B. M. et al. In vitro and in vivo efficacy of tecovirimat against a recently emerged 2022 monkeypox virus isolate. *Sci. Transl. Med.* **14**, eade7646 (2022).
39. O'Laughlin, K. et al. Clinical use of tecovirimat (Tpoxx) for treatment of monkeypox under an investigational new drug protocol—United States, May–August 2022. *Morb. Mortal. Wkly Rep.* **71**, 1190–1195 (2022).
40. Govind, A. et al. Severe mpox infections in people with uncontrolled human immunodeficiency virus (HIV). *Clin. Infect. Dis.* **76**, 1843–1846 (2023).
41. McLean, J. et al. Tecovirimat treatment of people with HIV during the 2022 mpox outbreak: a retrospective cohort study. *Ann. Intern. Med.* **176**, 642–648 (2023).
42. Hutson, C. L. & Damon, I. K. Monkeypox virus infections in small animal models for evaluation of anti-poxvirus agents. *Viruses* **2**, 2763–2776 (2010).
43. Xuan, D. T. M. et al. Comparison of transcriptomic signatures between monkeypox-infected monkey and human cell lines. *J. Immunol. Res* **2022**, 3883822 (2022).
44. Zhang, M. et al. Recessive cardiac phenotypes in induced pluripotent stem cell models of Jervell and Lange–Nielsen syndrome: disease mechanisms and pharmacological rescue. *Proc. Natl Acad. Sci. USA* **111**, E5383–E5392 (2014).
45. Bajanca, F., Luz, M., Duxson, M. J. & Thorsteinsdottir, S. Integrins in the mouse myotome: developmental changes and differences between the epaxial and hypaxial lineage. *Dev. Dyn.* **231**, 402–415 (2004).
46. Chen, S., Zhou, Y., Chen, Y. & Gu, J. fastp: an ultra-fast all-in-one FASTQ preprocessor. *Bioinformatics* **34**, i884–i890 (2018).
47. Li, H. & Durbin, R. Fast and accurate short read alignment with Burrows-Wheeler transform. *Bioinformatics* **25**, 1754–1760 (2009).
48. UCSC Genome Browser on Human (GRCh38/hg38). *UCSC* https://genome.ucsc.edu/cgi-bin/hgTracks?db=hub_3471181_GCF_014621545.1 (2023).
49. Danecek, P. et al. Twelve years of SAMtools and BCFtools. *Gigascience* **10**, giab008 (2021).

Acknowledgements

We thank our colleagues at the hiPSC Hotel, Leiden University Medical Center, for providing hiPS cell lines. This work was supported by a VIDI grant (grant number 91719300) from the Dutch Research Council (NWO) to Q.P., and by the Novo Nordisk Foundation Center for Stem Cell Medicine supported by the Novo Nordisk Foundation, Denmark (grant number NNF21CC0073729) to K.R. K.R. is Chargé de Recherche at the Institut National de la Santé et de la Recherche Médicale (INSERM).

Author contributions

P.L., S.T.P., K.R. and Q.P. conceptualized the project. G.X., R.S., R.I. and I.A. developed the methodology. P.L., S.T.P., K.R., A.C.V. and Q.P. conducted the investigations. P.L., S.T.P., R.I., I.A. and K.R. conducted formal analysis. P.L., S.T.P., K.R. and Q.P. wrote the original draft. A.C.V., M.J.B. and M.P.P. reviewed and edited the manuscript. K.R. and Q.P. acquired funding.

Competing interests

The authors declare no competing interests.

Additional information

Extended data is available for this paper at https://doi.org/10.1038/s41564-023-01489-6.

Supplementary information The online version contains supplementary material available at https://doi.org/10.1038/s41564-023-01489-6.

Correspondence and requests for materials should be addressed to Karine Raymond or Qiuwei Pan.

Peer review information *Nature Microbiology* thanks David Ulaeto, Karl Koehler and the other, anonymous, reviewer(s) for their contribution to the peer review of this work.

https://doi.org/10.1038/s41564-023-01489-6

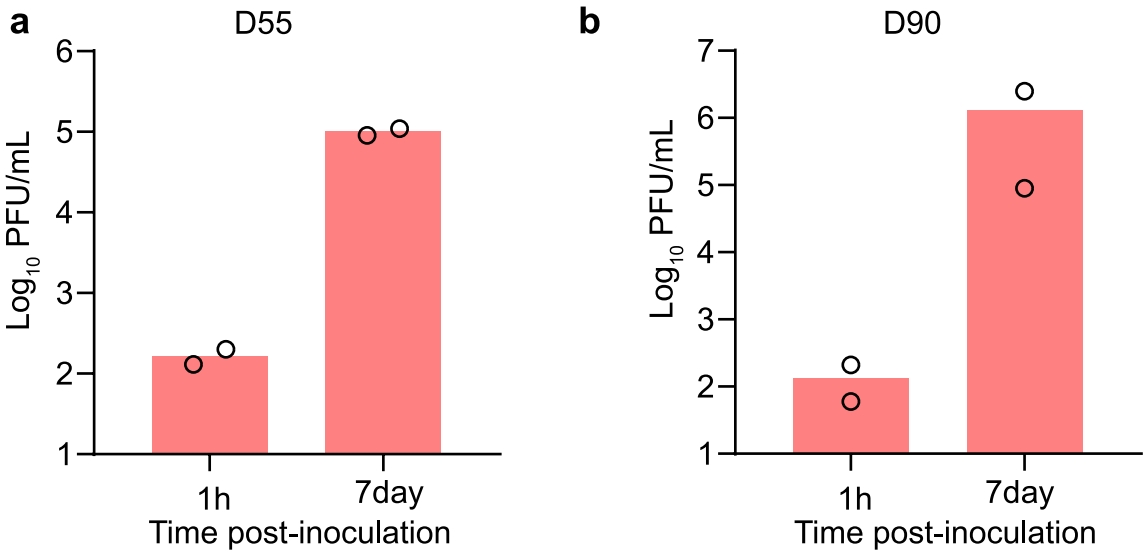

Extended Data Fig. 1 | Quantification of infectious viral titers in organoids at 1 hour and 7 days post-inoculation. a, Infectious viral titers of organoids after 55 days of differentiation (n = 2 biological replicates). **b**, Infectious viral titers of organoids after 90 days of differentiation (n = 2 biological replicates).

https://doi.org/10.1038/s41564-023-01489-6

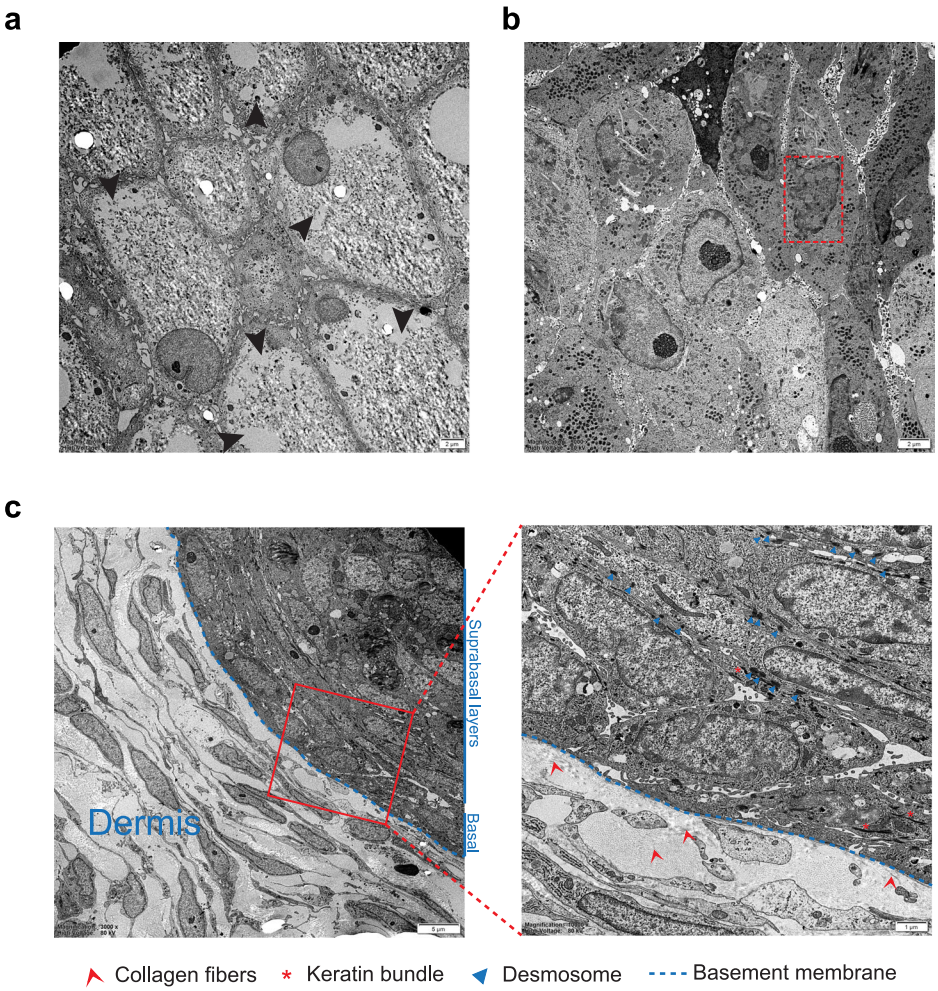

Extended Data Fig. 2 | Transmission electron microscopy analysis of skin organoids. (**a**) and (**b**) show destroyed organelles, degrading cytoplasm (black arrowheads), and irregular chromatin condensation, alteration of nucleus membrane (red frame) in end-stage skin organoids. **c**, Representative skin characteristics was visualized in ALI-skin organoid, including skin dermis, collagen fibers, keratin bundles, desmosomes, and basement membrane.

https://doi.org/10.1038/s41564-023-01489-6

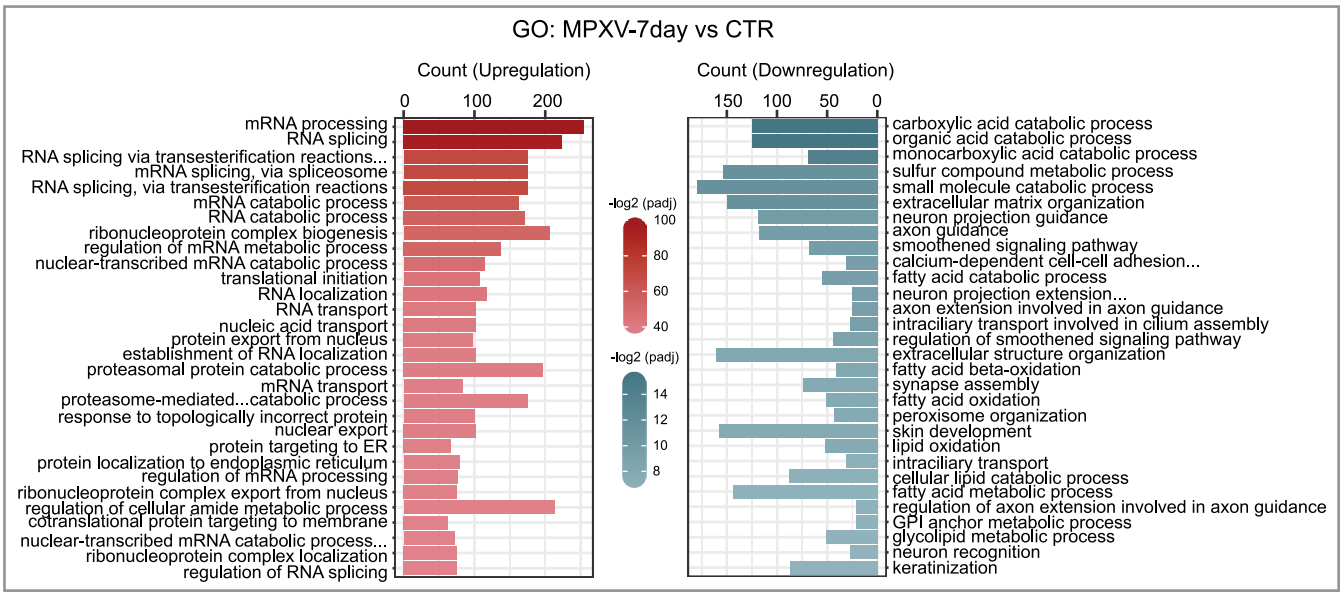

Extended Data Fig. 3 | Gene ontology analysis of skin organoids upon MPXV infection. Top 30 significantly up- and down-regulated pathways by gene ontology analysis at day 7 post-inoculation, compared with the uninfected group. Three independent skin organoids were used in each group, *P* value determined by DESeq2.

https://doi.org/10.1038/s41564-023-01489-6

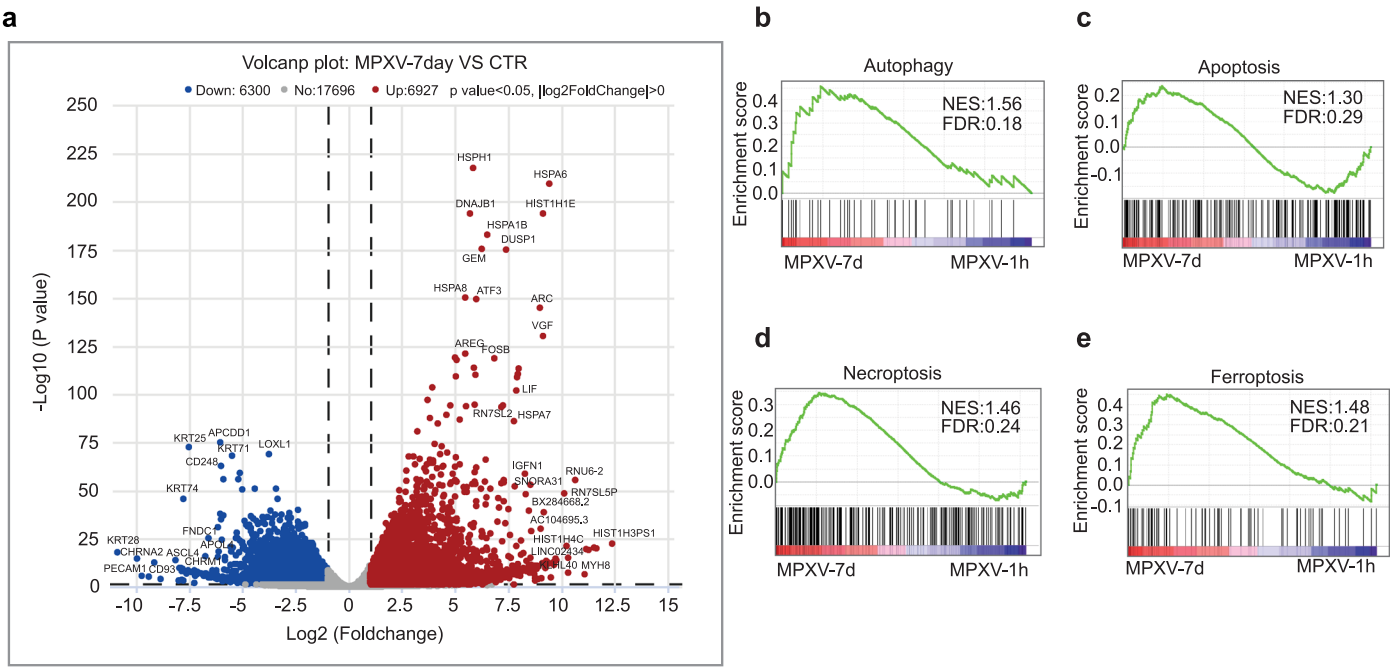

Extended Data Fig. 4 | Transcriptomic analysis of skin organoids upon 7 days infection, compared with uninfected or 1 h infection group. a, Significantly up- and down-regulated genes by volcano plot analysis at day 7 post-inoculation, compared with the uninfected group. *P* value determined by DESeq2. **b-e**, Gene set enrichment analysis (GSEA) of KEGG pathways including autophagy_other (HSA04136), apoptosis (HSA04210), necroptosis (HSA04217), and ferroptosis (HSA04216) in skin organoids.

https://doi.org/10.1038/s41564-023-01489-6

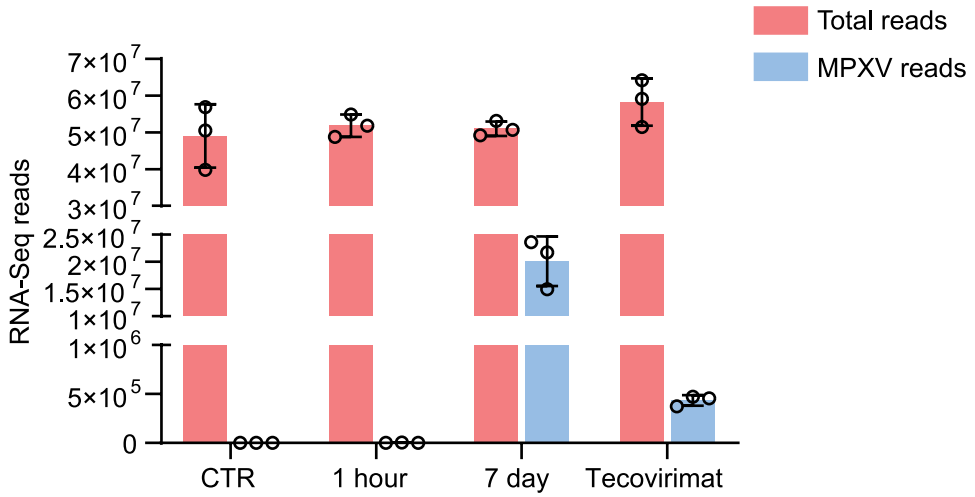

Extended Data Fig. 5 | Total reads and mapped MPXV reads in different skin organoid groups by bulk-RNA sequencing. Skin organoids were either not infected (control), infected for 1 hour (1 hour), infected for 7 days (7 day) or infected and treated with 5 µM of tecovirimat for 7 days (Tecovirimat), n = 3 per group. Data are presented as means of biological replicates ± SEM.

https://doi.org/10.1038/s41564-023-01489-6

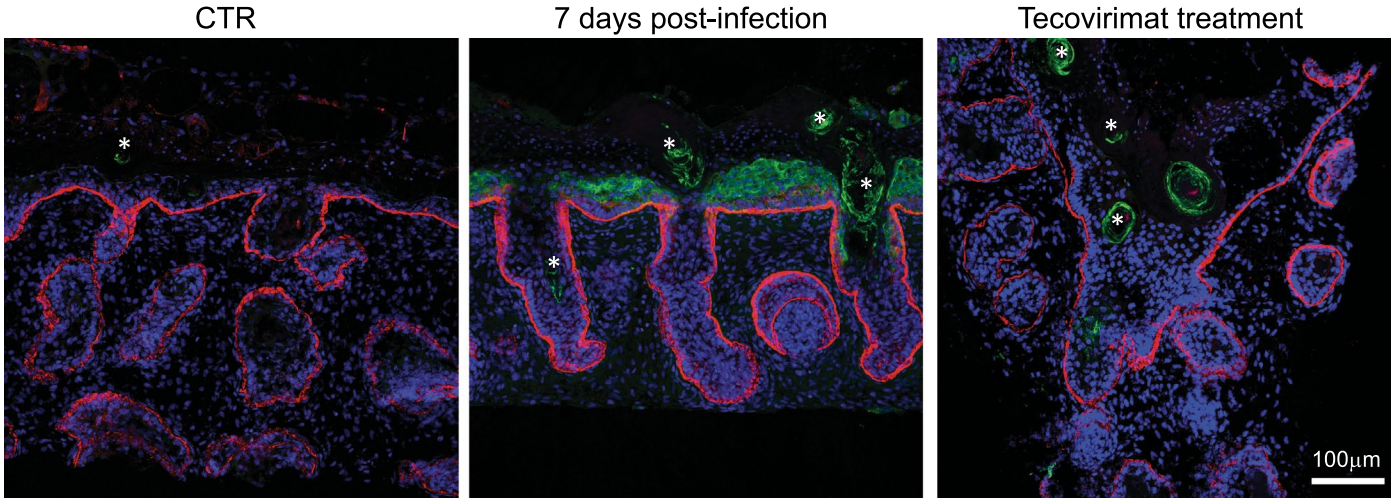

Extended Data Fig. 6 | Low magnification images of the mpox virion (green) and integrin β4 subunit (red) immunostaining depicted in Fig. 6g. White * indicates the potential autofluorescent signal of the cornified layer of the epithelium, which is distinguishable from the specific staining of mpox virion observed in the conditions where MPXV had been inoculated.